

Supporting Information

See-Saw Ni(II) thiosemicarbazones, Energy and Photophysical Properties

Satyendra Verma,^a Jitendra Nath,^b Jubaraj B. Baruah^{a*}

Content list

Figure 1S	High-resolution mass of the complex 1 (inset has the respective calculated mass pattern)
Figure 2S	High-resolution mass of the complex 2 (inset has the respective calculated mass pattern)
Figure 3S	High-resolution mass of the complex 3 (inset has the respective calculated mass pattern)
Figure 4S	IR spectra of the nickel complexes (a) complex 1 , (b) complex 2 , and (c) complex 3 (on the right side is the expanded region showing peaks appearing between 500-1500 cm ⁻¹)
Figure 5S	¹ HNMR (400 MHz, CDCl ₃) spectra of Complex 2
Figure 6S	¹ HNMR (400 MHz, CDCl ₃) spectra of Complex 3
Figure 7S	Comparison ¹ HNMR (400 MHz, CDCl ₃ / DMSO-d ₆) spectra of 23CIHATU ligand and complex 1 (on top expanded aromatic region)
Figure 8S	Comparison ¹ H NMR (400 MHz, CDCl ₃ / DMSO-d ₆) spectra of Ligand OMeHATU and complex 2 (Top is expanded spectra).
Figure 9S	Fingerprint plots from the Hirshfeld analyses of the complexes (a) 1 , (b) 2 , and (c) 3
Figure 10S	Powder XRD patterns of Ni(24CIATU) ₂ (complex 3)
Figure 11S	Figure 5S: Powder XRD patterns of Ni(24CIATU) ₂ (Complex 3)
Figure 12S	Comparison of the dual emissions of the complexes 2 and 3 recorded in CHCl ₃ (λ _{ex} = 300 nm)
Figure 13S	Time-dependent fluorescence spectra Ni(3OMeATU) ₂ (complex 1) (λ _{ex} = 300 nm, solvent CHCl ₃ , Concentration 3.3 μM)
Figure 14S	Time-dependent fluorescence spectra Ni(23CIATU) ₂ (complex 2) (λ _{ex} = 300 nm, solvent CHCl ₃ , Concentration 3.3 μM)
Figure 15S	Comparison of fluorescence spectra of (a) 23CIHATU (ligand) and (b) complex 2 , Ni(23CIATU) ₂ in CHCl ₃ (λ _{ex} = 400 nm, solvent CHCl ₃ , concentration 3.3 μM)
Figure 16S	Time-dependent fluorescence spectra Complex 1 , Ni(3OMeATU) ₂ . (λ _{ex} = 400 nm, solvent CHCl ₃ , Concentration 3.3 μM)
Figure 17S	Time-dependent fluorescence spectra Ni(24CIATU) ₂ (complex 3) (λ _{ex} = 400 nm solvent CHCl ₃ , Concentration 3.3 μM)
Figure 18S	Time-dependent fluorescence spectra Ni(23CIATU) ₂ (complex 2) (λ _{ex} = 400 nm, solvent CHCl ₃ , Concentration 3.3 μM)
Figure 19S	Variable temperature ¹ H NMR (400 MHz, CDCl ₃ : DMSO-d ₆ 1:1) spectra of ligand 24CIHATU (a, b, c, d, e, f at -20, -10, 0, 10, 20, 25, respectively)
Figure 20S	The dispersion corrected energy associated with the isomers of the complexes 1-3 , the observed form is highlighted by encircled dots
Figure 21S	Theoretically calculated change in the energy of complex 2 with different dihedral angles C40-C39-N6-C38. Calculations were done by DFT at the B3LYP functional level using LANL2DZ as the basis set
Figure 22S	Theoretically calculated change in the energy of complex 3 with different dihedral angles C40-C39-N6-C38. Calculations were done by DFT at the B3LYP functional level using LANL2DZ as the basis set
Figure 23S	Microscopic images of crystals (a) complex 1 and (b) complex 2
Table 1S	Crystal and refinement data of the complexes
Table 2S	Hydrogen bond parameters of the complexes

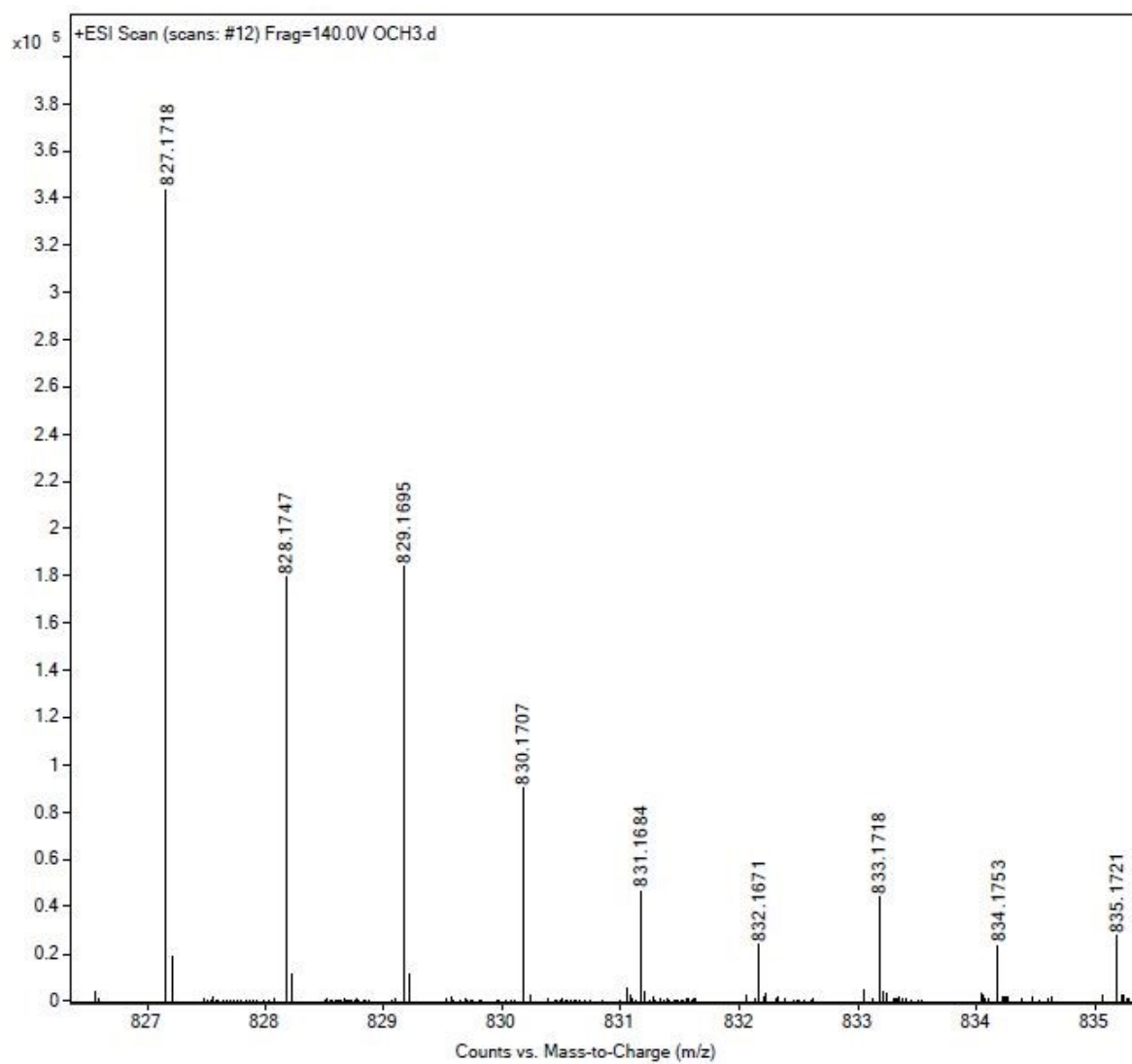


Figure 1S: High-resolution mass of the complexes **1** (inset has the respective calculated mass pattern).

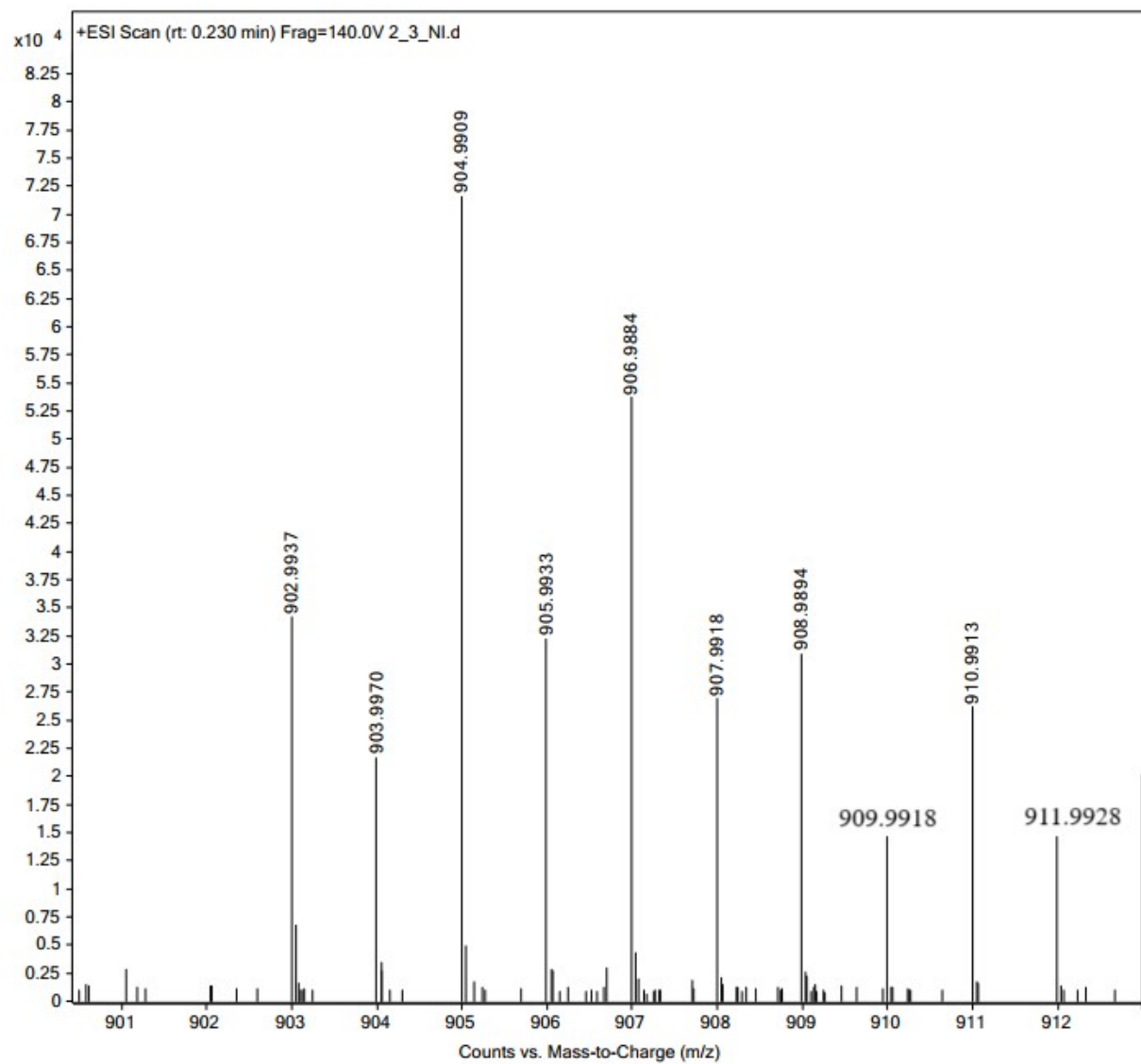
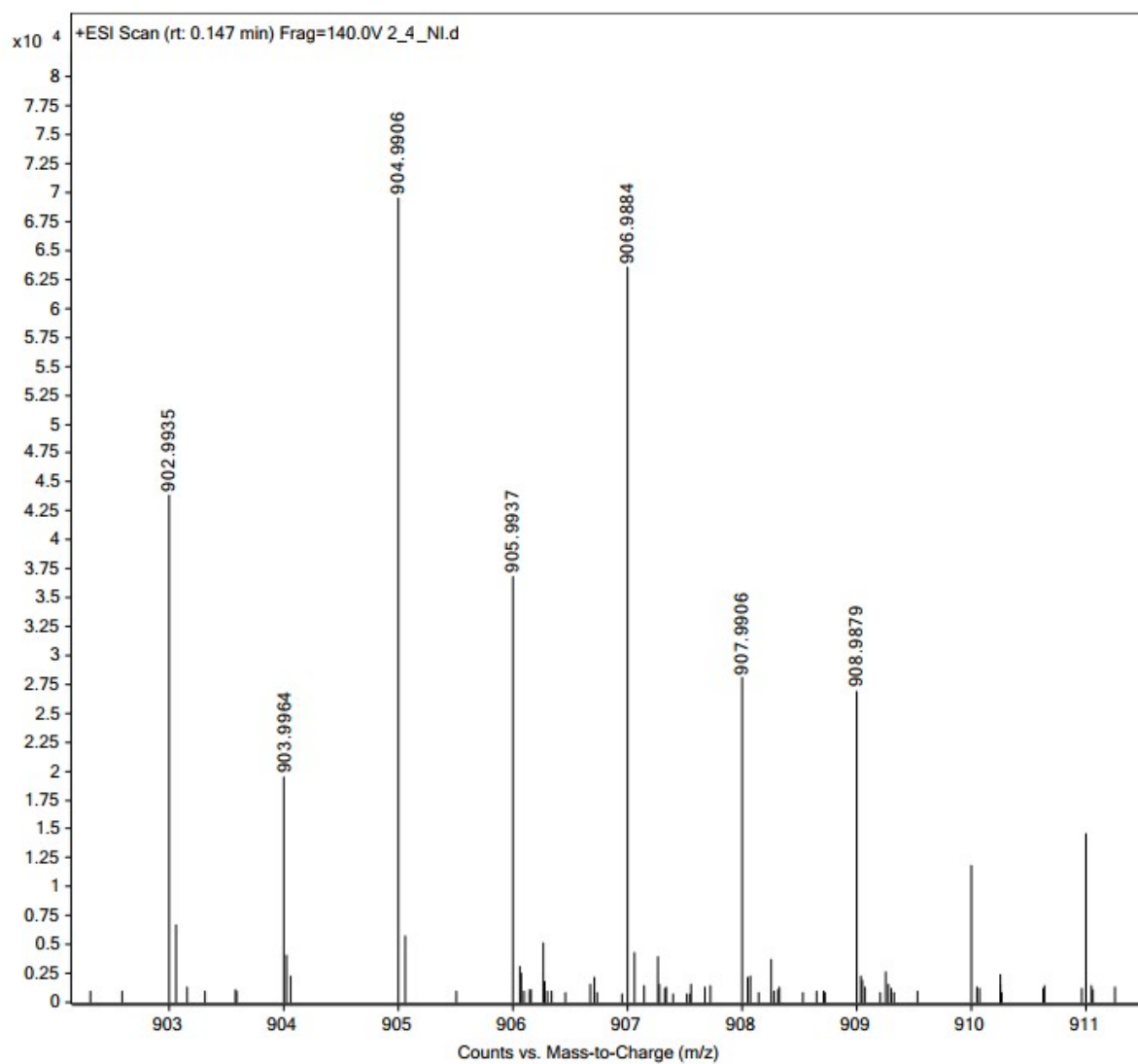
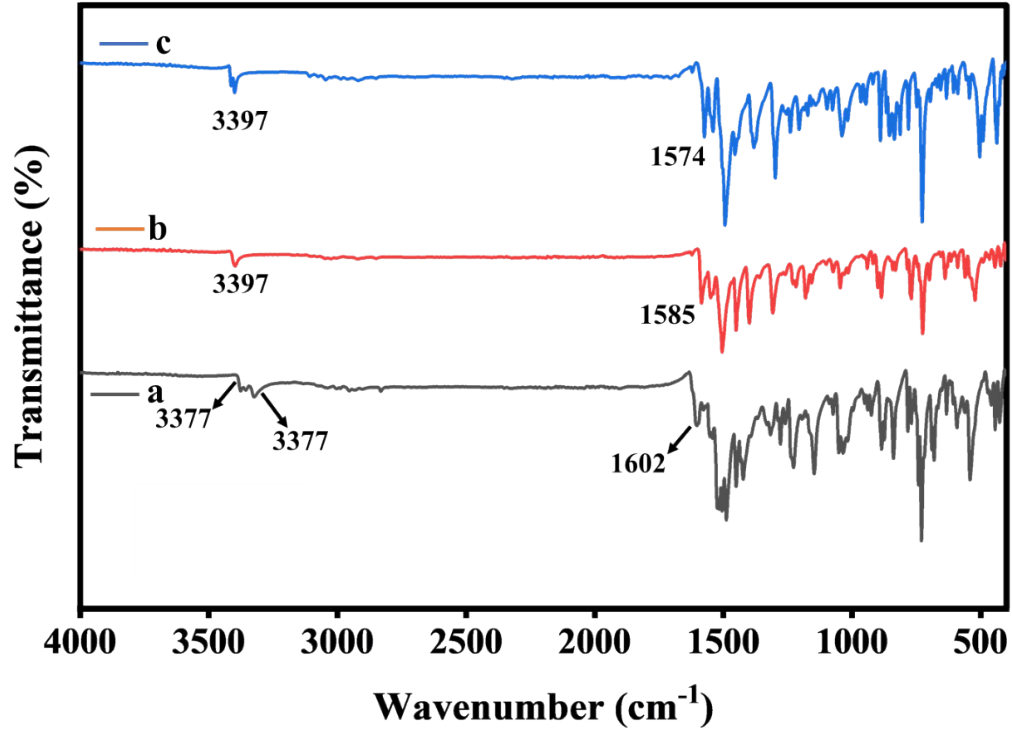


Figure 2S: High-resolution mass of the complexes **2** (inset has the respective calculated mass pattern).

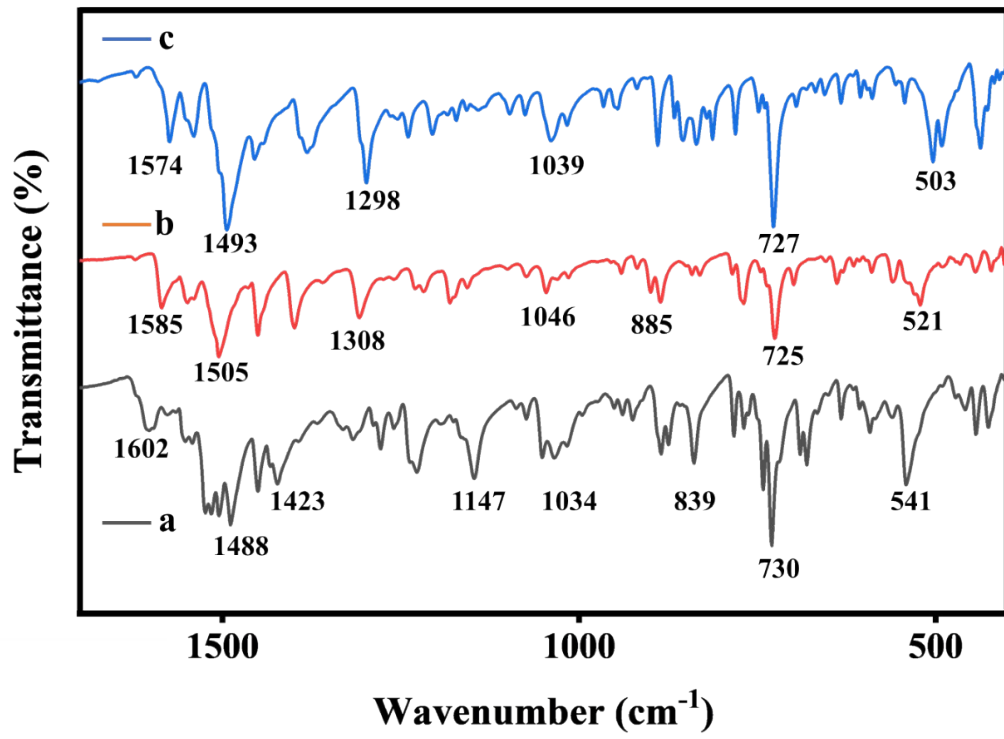


(c)

Figure 3S: High-resolution mass of the complexes **3** (inset has the respective calculated mass pattern).



(a)



(b)

Figure 4S: IR spectra of the nickel complexes (a) complex **1**, (b) complex **2**, and (c) complex **3** (on the right side is the expanded region showing peaks appearing between 500-1500 cm^{-1}).

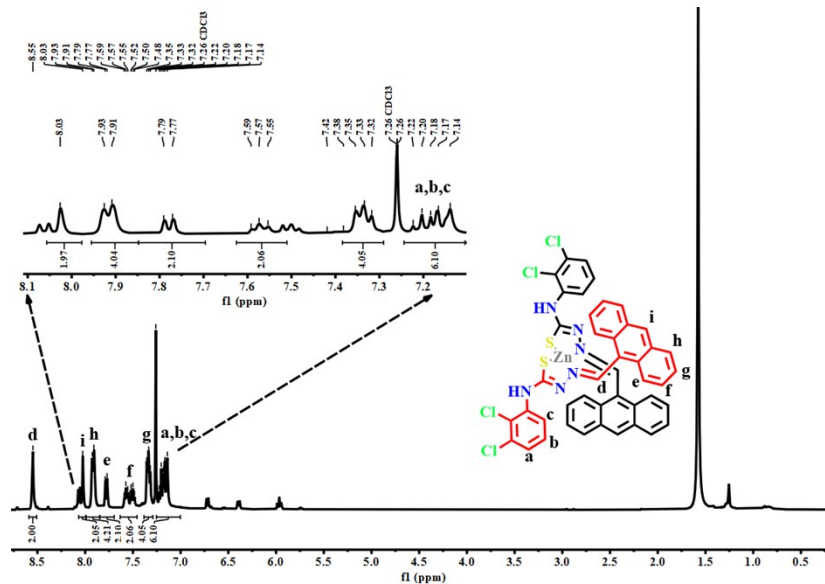


Figure 5S: $^1\text{H NMR}$ (400 MHz, CDCl_3) spectra of Complex **2**

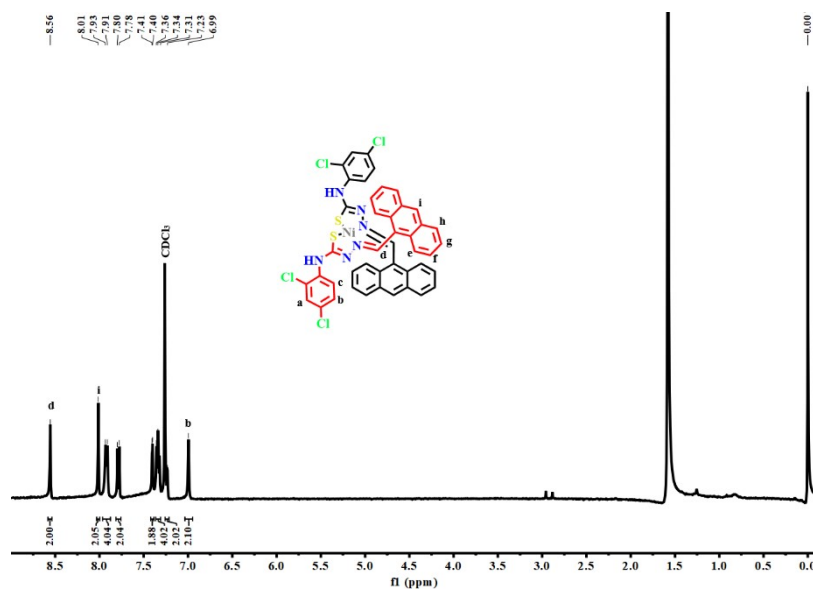


Figure 6S: $^1\text{H NMR}$ (400 MHz, CDCl_3) spectra of Complex **3**

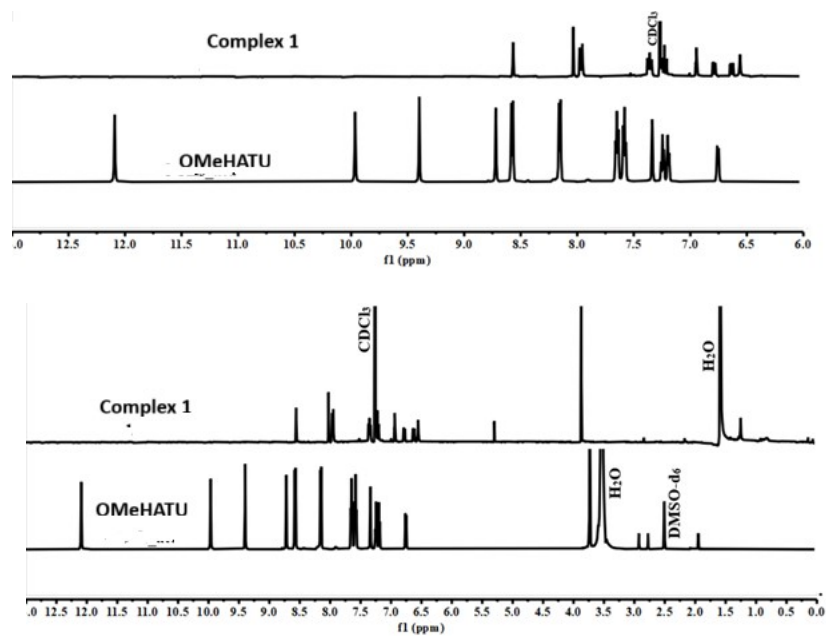


Figure 7S: Comparison ^1H NMR (400 MHz, $\text{CDCl}_3/\text{DMSO-d}_6$) spectra of Ligand OMeHATU and complex 1 (Top is expanded spectra).

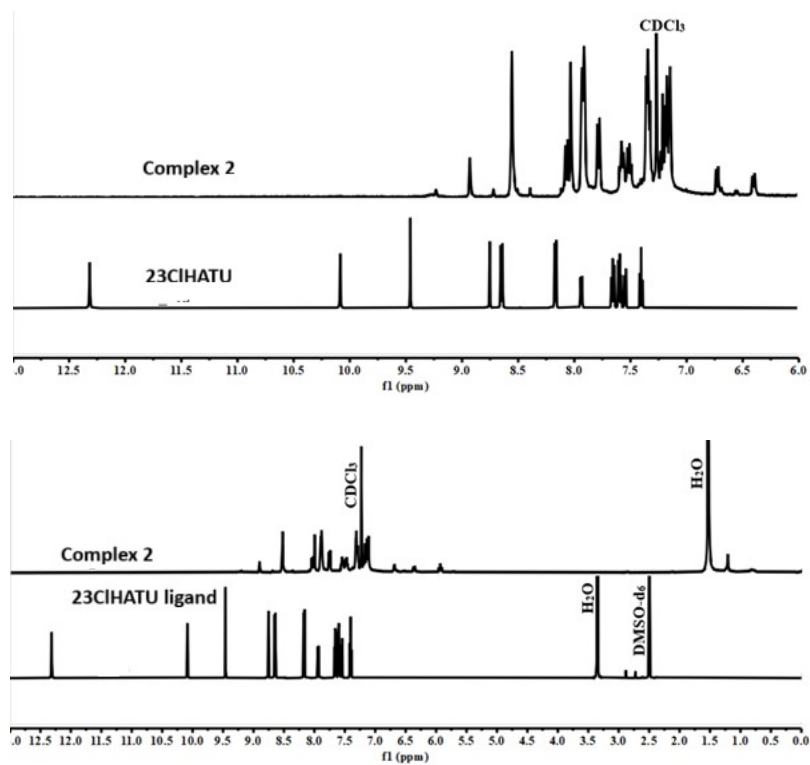


Figure 8S: Comparison ^1H NMR (400 MHz, $\text{CDCl}_3/\text{DMSO-d}_6$) spectra of 23CIHATU ligand and complex 2 (on top expanded aromatic region).

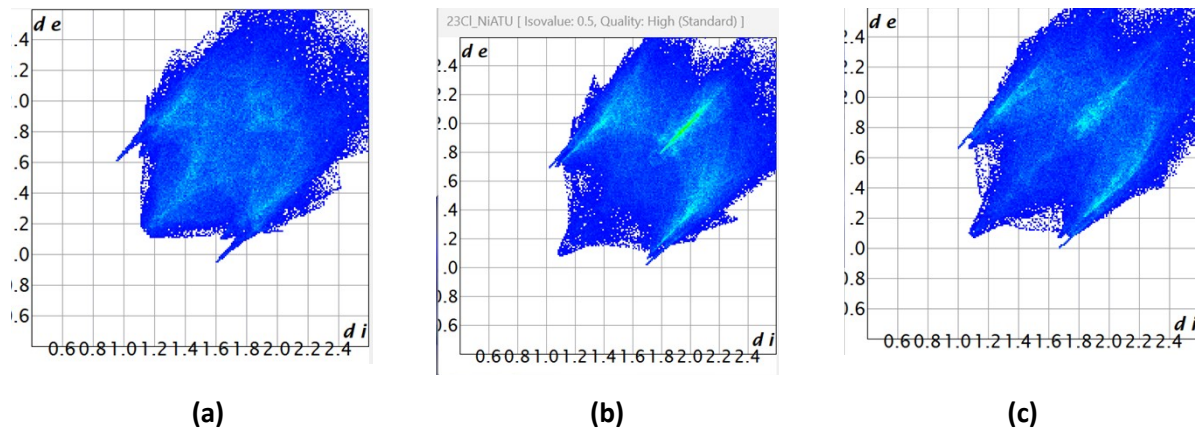


Figure 9S: Fingerprint plots from the Hirshfeld analyses of the complexes (a) **1**, (b) **2**, and (c) **3**.

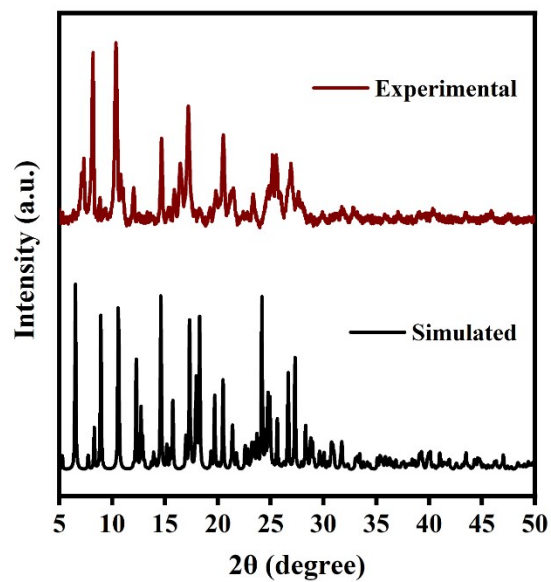


Figure 10S: Powder XRD patterns of $\text{Ni}(\text{23ClATU})_2$ (complex 2)

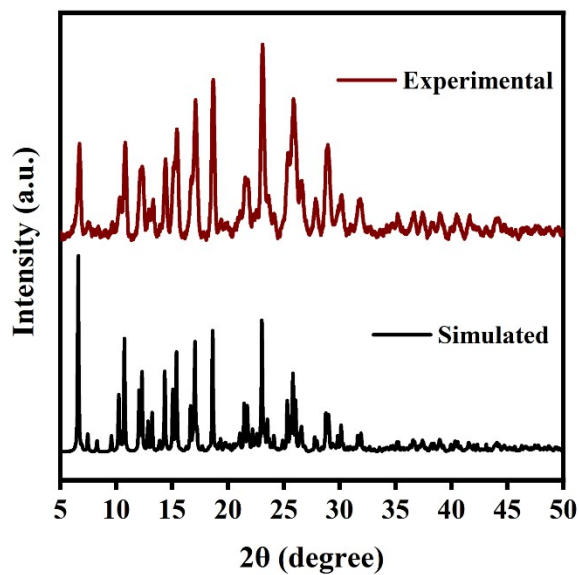


Figure 11S: Powder XRD patterns of Ni(24ClATU)₂ (Complex 3)

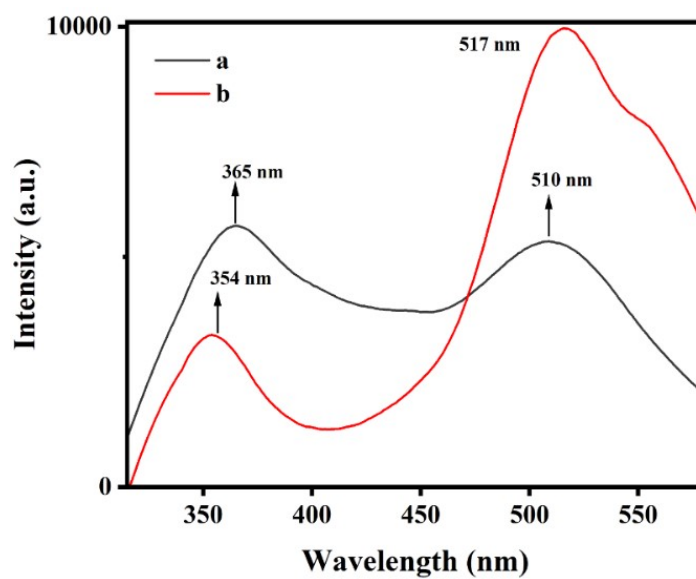


Figure 12S: Comparison of the dual emissions of the complexes 2 and 3 recorded in CHCl₃ (λ_{ex} = 300 nm, concentration 200 μM)

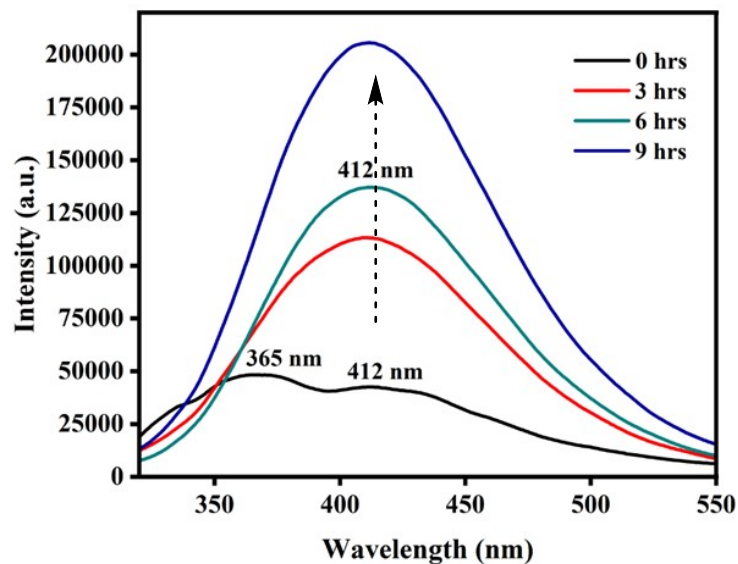


Figure 13S: Time-dependent fluorescence spectra Ni(3OMeATU)₂ (Complex 1) ($\lambda_{\text{ex}} = 300 \text{ nm}$, solvent CHCl₃, concentration 3.3 μM).

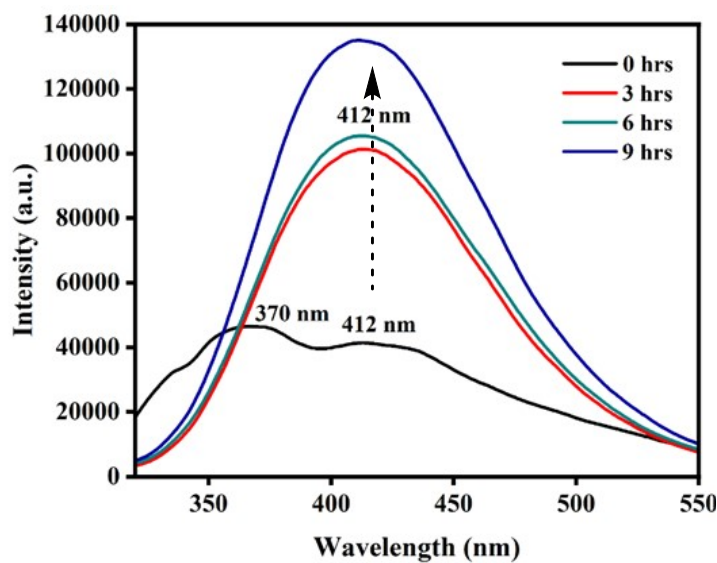


Figure 14S: Time-dependent fluorescence spectra Ni(23ClATU)₂ (complex 2) ($\lambda_{\text{ex}} = 300 \text{ nm}$, solvent CHCl₃, concentration 3.3 μM).

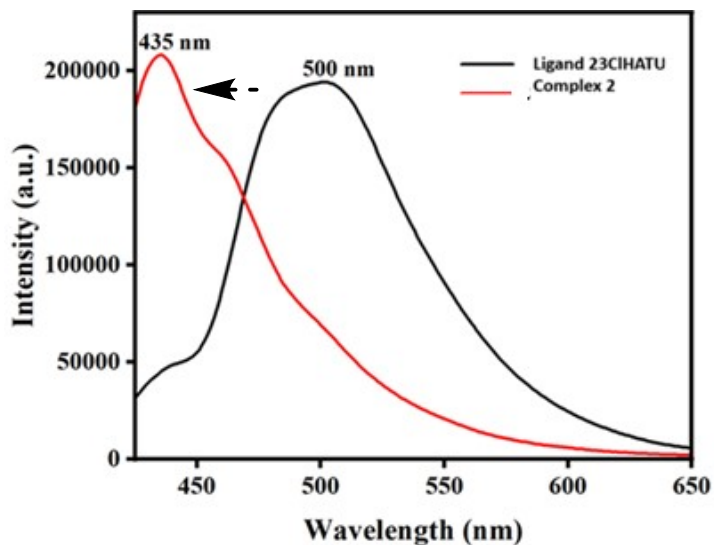


Figure 15S: Comparison of fluorescence spectra of (a) 23CIHATU (ligand) and (b) complex 2, Ni(23CIATU)₂ in CHCl₃ (λ_{ex} = 400 nm, solvent CHCl₃, concentration 3.3 μM)

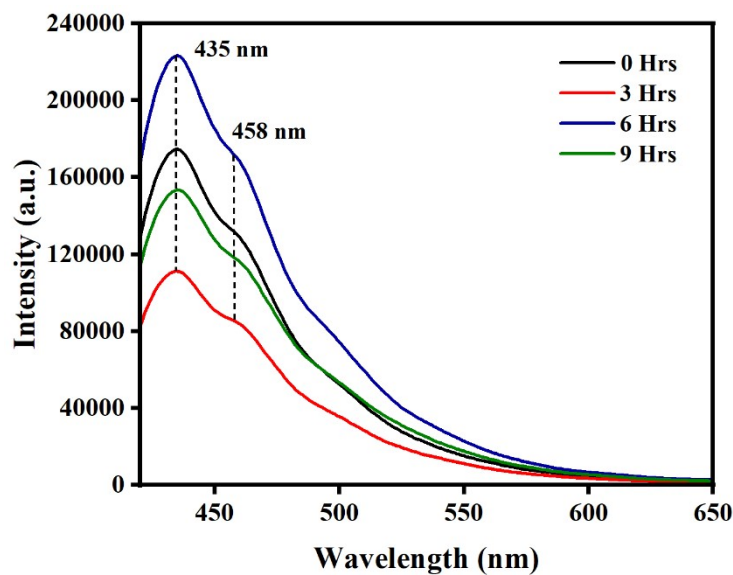


Figure 16S: Time-dependent fluorescence spectra complex 1, Ni(3OMeATU)₂ (λ_{ex} = 400 nm, solvent CHCl₃, concentration 3.3 μM)

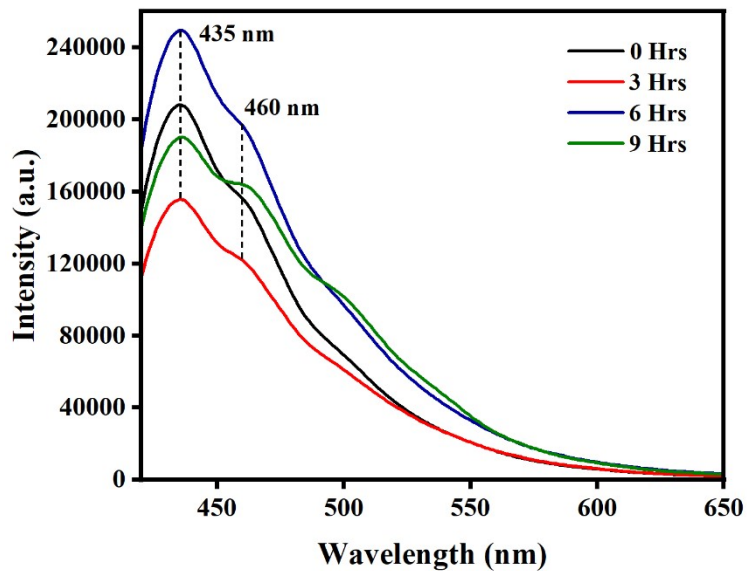


Figure 17S: Time-dependent fluorescence spectra Ni(24ClATU)₂ (complex 3) ($\lambda_{\text{ex}}=400$ nm solvent CHCl₃, concentration 3.3 μM)

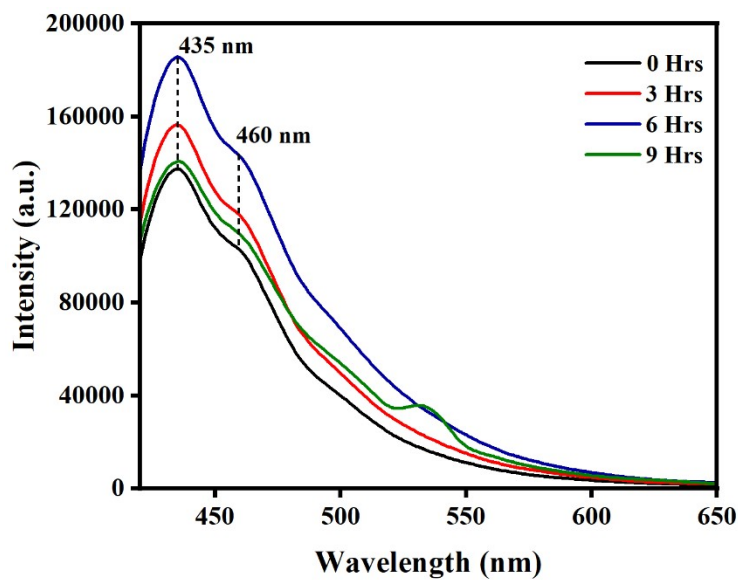


Figure 18S: Time-dependent fluorescence spectra Ni(23ClATU)₂ (complex 2) ($\lambda_{\text{ex}}=400$ nm, solvent CHCl₃, concentration 3.3 μM)

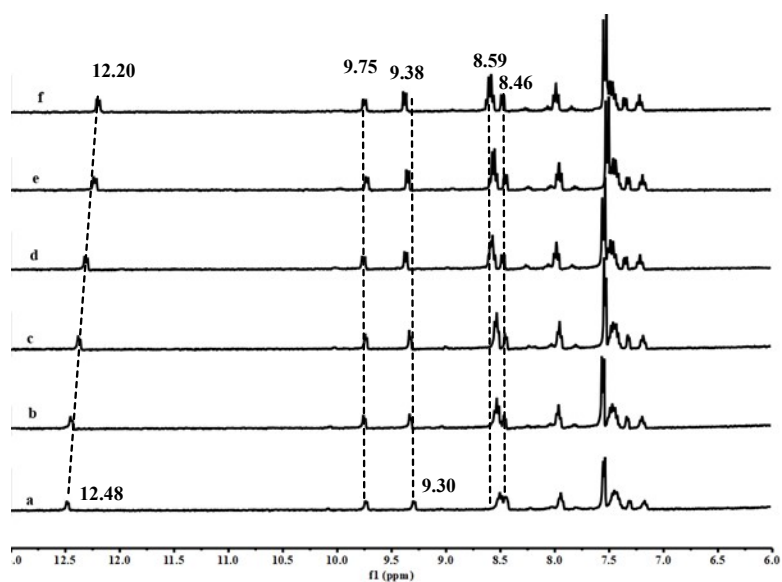


Figure 19S: Variable temperature ^1H NMR (400 MHz, CDCl_3 : DMSO-d_6 1:1) spectra of ligand 24CIHATU. (a, b, c, d, e, f at -20 , -10 , 0 , 10 , 20 , 25 , respectively)

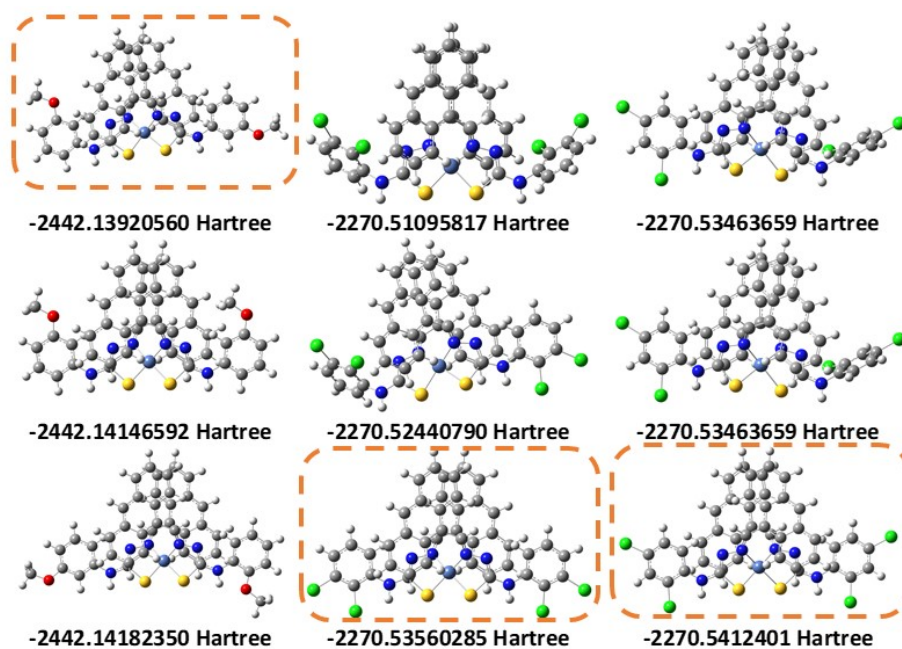


Figure 20S: The dispersion corrected energy associated with the isomers of the complexes 1-3, the observed form is highlighted by encircled dots

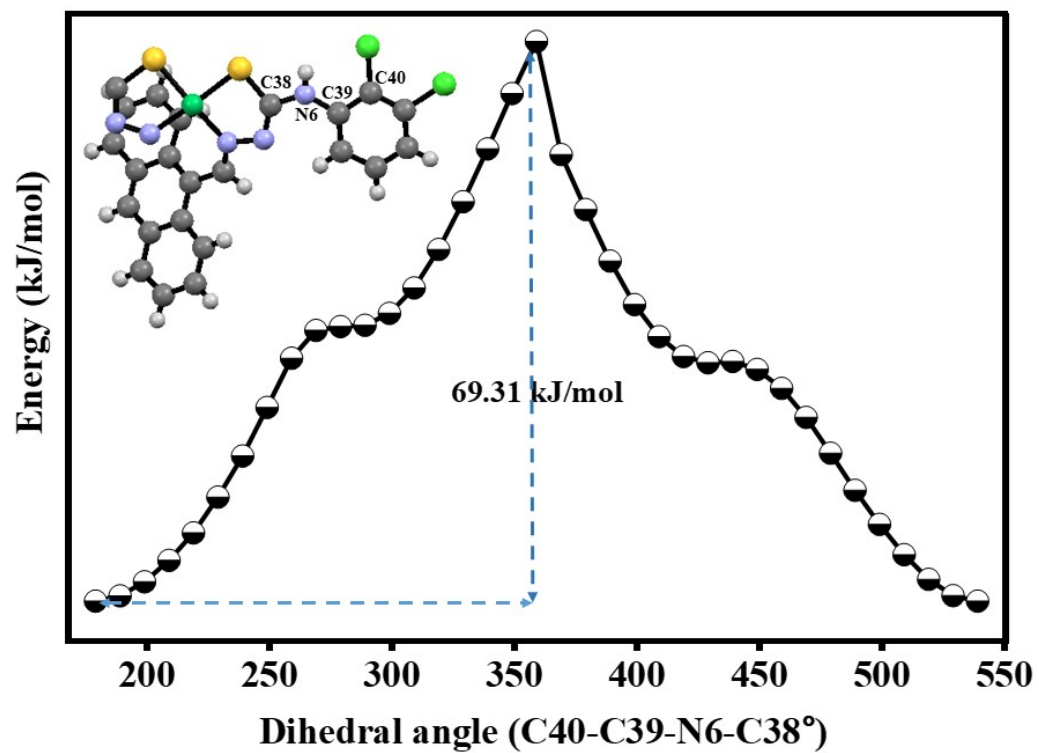


Figure 21S: Theoretically calculated change in the energy of complex 2 with different dihedral angles C40-C39-N6-C38. Calculations were done by DFT at the B3LYP functional level using LANL2DZ as the basis set

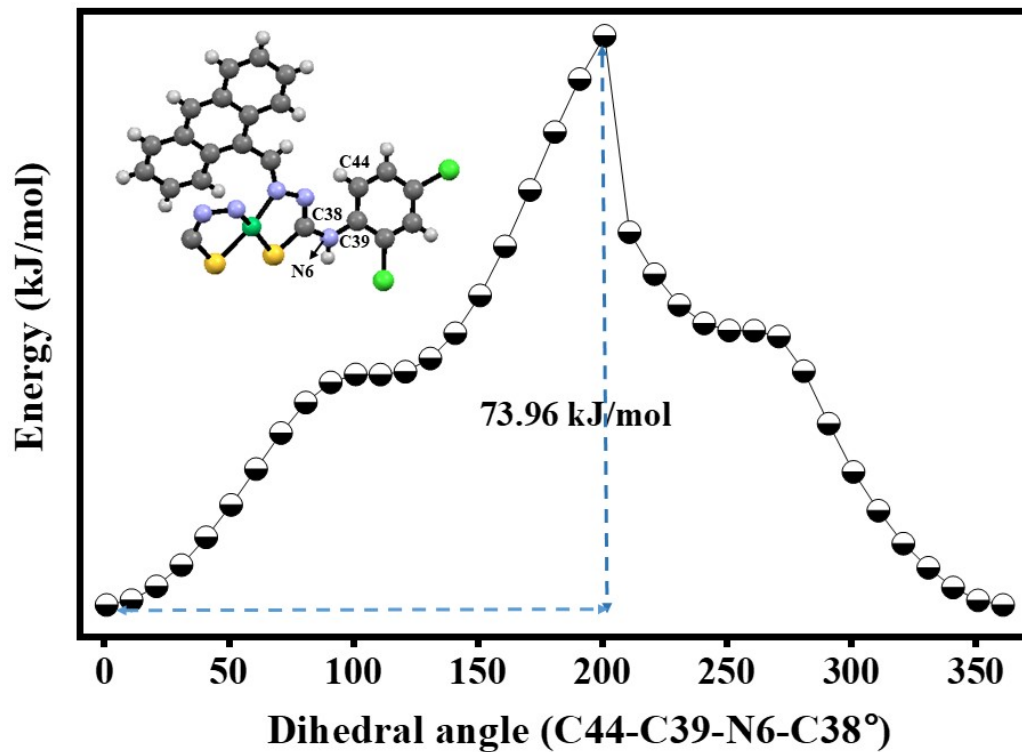
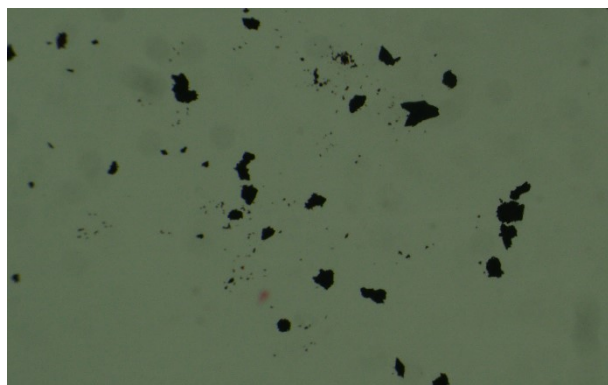
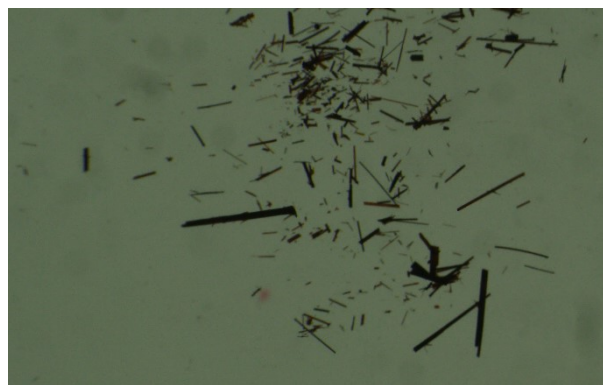


Figure 22S: Theoretically calculated change in the energy of complex 3 with different dihedral angles C44-C39-N6-C38. Calculations were done by DFT at the B3LYP functional level using LANL2DZ as the basis set



(a)



(b)

Figure 23S: Microscopic images of crystals (a) complex 1 and (b) complex 2

Table 1S: Crystal and refinement data of the complexes

Parameter	Complex 1	Complex 2	Complex 3
Formula	C ₄₆ H ₃₆ N ₆ O ₂ S ₂ Ni	C ₄₅ H ₂₉ N ₆ Cl ₇ S ₂ Ni	C ₄₄ H ₂₈ N ₆ S ₂ Cl ₄ Ni
Mol. wt.	827.64	1024.72	905.35
Space group	<i>Pbca</i>	<i>P2₁/n</i>	<i>P2₁/c</i>
a(Å)	11.0335(4)	7.6501(14)	13.4028(16)
b(Å)	21.1887(8)	27.110(5)	25.516(3)
c(Å)	33.5173(13)	21.294(4)	11.7627(14)
α(°)	90	90	90
β(°)	90	90.173(6)	91.750(4)
γ(°)	90	90	90
V(Å ³)	7835.9(5)	4416.2(14)	4020.8(8)
Density, g cm ⁻³	1.403	1.541	1.496
Abs. coeff., mm ⁻¹	0.650	0.999	0.894
F(000)	3440	2080	1848
Total no. of reflections	6884	7582	7108
Reflections, I > 2σ(I)	4206	3991	4834
Max. θ/°	24.998	24.8	25.049
Ranges (h, k, l)	-13 ≤ h ≤ 13 25 ≤ k ≤ 25 -39 ≤ l ≤ 39	-9 ≤ h ≤ 9 -31 ≤ k ≤ 31 -23 ≤ l ≤ 25	-15 ≤ h ≤ 15 -30 ≤ k ≤ 30 -13 ≤ l ≤ 14
Completeness to 2θ (%)	99.9	99.9	99.9
Data/restraints/parameters	6884/2/516	7582/0/550	7108/0/514
Goof (F ²)	1.042	1.032	1.059
R indices [I > 2σ(I)]	0.0611	0.0785	0.0440
wR ₂ [I > 2σ(I)]	0.1314	0.1685	0.0862
R indices (all data)	0.1175	0.1634	0.0798
wR ₂ [all data]	0.1519	0.2015	0.0948
CCDC No.	2346244	2346249	2346251

Table 2S: Hydrogen bond parameters of the complexes

Compounds	D-H...A	d _{D-H} (Å)	d _{H...A} (Å)	d _{D...A} (Å)	∠D-H...A (°)
Complex 1	N(6)–H(6)...S(1) [1/2+x,y,1/2-z]	0.93	2.71	3.539(4)	162
	C(2)–H(2)...N(1) [x,y,z]	0.93	2.55	3.066(6)	115
	C(22)–H(22)...N(2)[x,y,z]	0.93	2.33	2.937(6)	122
	C(35)–H(35)...N(4) [x,y,z]	0.93	2.54	3.086(5)	118
	C(41)–H(41)...N(5) [x,y,z]		2.34	2.926(6)	121
Complex 2	N(3)–H(3)...Cl(1) [x,y,z]	0.86	2.44	2.911(6)	115
	N(3)–H(6)...Cl(3) [x,y,z]	0.86	2.45	2.91 (6)	115
	C(12)–H(12)...N(1) [x,y,z]	0.93	2.51	3.055(9)	118
	C(22)–H(22)...N(2) [x,y,z]	0.93	2.28	2.891(4)	122
	C(24)–H(24)...N(4) [x,y,z]	0.93	2.57	3.105(10)	117
	C(44)–H(44)...N(5) [x,y,z]	0.93	2.29	2.897 (10)	122
	C(45)–H(45)...S(1) [1+x,y,z]	0.98	2.82	3.777 (11)	166
Complex 3	N(3)–H(3)...Cl(1) [x,y,z]	0.86	2.51	2.939(3)	122
	N(6)–H(6)...Cl(3) [x,y,z]	0.86	2.53	2.941(3)	110
	C(2)–H(2)...N1(4) [x,y,z]	0.93	2.58	3.107 (5)	116
	C(22)–H(22)...N(2) [x,y,z]	0.93	2.31	2.879 (5)	119
	C(34)–H(34)...N(4) [x,y,z]	0.93	2.58	3.159 (4)	121
	C(37)–H(37)...S(2)[x,1/2-y,-1/2+z]	0.93	2.82	3.753 (3)	177
	C(44)–H(44)...N(5) [x,y,z]	0.93	2.31	2.856 (4)	117

